LETTER

doi:10.1038/nature17950

Noncanonical autophagy inhibits the autoinflammatory, lupus-like response to dying cells

Jennifer Martinez[1,2], Larissa D. Cunha[1], Sunmin Park[3], Mao Yang[1], Qun Lu[3], Robert Orchard[3], Quan-Zhen Li[4], Mei Yan[4], Laura Janke[1], Cliff Guy[1], Andreas Linkermann[5], Herbert W. Virgin[3] & Douglas R. Green[1]

Defects in clearance of dying cells have been proposed to underlie the pathogenesis of systemic lupus erythematosus (SLE)[1]. Mice lacking molecules associated with dying cell clearance develop SLE-like disease[2], and phagocytes from patients with SLE often display defective clearance and increased inflammatory cytokine production when exposed to dying cells *in vitro*. Previously, we[3–6] and others[7] described a form of noncanonical autophagy known as LC3-associated phagocytosis (LAP), in which phagosomes containing engulfed particles, including dying cells[3,4,7], recruit elements of the autophagy pathway to facilitate maturation of phagosomes and digestion of their contents. Genome-wide association studies have identified polymorphisms in the *Atg5* (ref. 8) and possibly *Atg7* (ref. 9) genes, involved in both canonical autophagy and LAP[3–7], as markers of a predisposition for SLE. Here we describe the consequences of defective LAP *in vivo*. Mice lacking any of several components of the LAP pathway show increased serum levels of inflammatory cytokines and autoantibodies, glomerular immune complex deposition, and evidence of kidney damage. When dying cells are injected into LAP-deficient mice, they are engulfed but not efficiently degraded and trigger acute elevation of pro-inflammatory cytokines but not anti-inflammatory interleukin (IL)-10. Repeated injection of dying cells into LAP-deficient, but not LAP-sufficient, mice accelerated the development of SLE-like disease, including increased serum levels of autoantibodies. By contrast, mice deficient in genes required for canonical autophagy but not LAP do not display defective dying cell clearance, inflammatory cytokine production, or SLE-like disease, and, like wild-type mice, produce IL-10 in response to dying cells. Therefore, defects in LAP, rather than canonical autophagy, can cause SLE-like phenomena, and may contribute to the pathogenesis of SLE.

LAP is a process in which some, but not all components of the autophagy machinery conjugate LC3 to phosphatidylethanolamine directly on the phagosome membrane[3,4,6,7,10]. The lipidated LC3 (LC3-II) then facilitates lysosomal fusion and cargo destruction. Both LAP and canonical autophagy require ATG7, ATG3, ATG5, ATG12, and ATG16L for LC3 lipidation[4,5]. However, unlike autophagy, LAP proceeds independently of the pre-initiation complex containing ULK1 and FIP200 (also known as RB1CC1)[3,4,6,7], and uses a distinct beclin 1 (BECN1) and VPS34 complex complex lacking ATG14 (ref. 5). By contrast, LAP, but not canonical autophagy, requires NADPH oxidase-2 (NOX2)[5], and rubicon (RUBCN)[5]. These requirements for LAP and canonical autophagy can therefore distinguish between the two processes (Supplementary Table 1). As many components of autophagy are required for development (for example, FIP200 (refs 11, 12) and BECN1 (ref. 12)) or post-natal survival (for example, ATG14 (refs 12, 13), ATG7 (ref. 12), ATG5 (ref. 12) and ATG16L (ref. 12)), we generated animals in which several autophagy genes were conditionally ablated using lysozyme M (LysM, also known as Lyz2)-Cre recombinase[14], affecting macrophages ($CD11b^+$ $F4/80^+$), monocytes ($CD11b^+$ $CD115^+$), some neutrophils ($CD11b^+$ $Ly6G^+$), and some conventional dendritic cells ($CD11b^+$ $CD11c^+$), but not eosinophils, plasmacytoid dendritic cells, or lymphocytes (Extended Data Fig. 1a, b). While all animals appeared normal at weaning, we observed that LAP-deficient genotypes failed to gain weight compared to their wild-type littermates (Fig. 1a). This effect was observed in animals lacking proteins required for both LAP and autophagy (ATG7, ATG5, BECN1) or LAP alone (NOX2, RUBCN), but not in animals lacking proteins required for autophagy but dispensable for LAP (FIP200, ULK1). Compared to LAP-sufficient animals, LAP-deficient mice displayed increased levels of circulating lymphocytes, monocytes and neutrophils (Extended Data Fig. 2a–c), with increased circulating activated $CD8^+$ T cells (Extended Data Fig. 2b, c), and augmented immunohistological staining of CD3 and Ki67 in the spleen (Extended Data Fig. 2d). Notably, LAP-deficient animals also contained increased serum levels of anti-double-stranded DNA (dsDNA) antibodies and anti-nuclear antibodies (Fig. 1b, c), as well as a broad array of antibodies against autoantigens commonly associated with SLE (Fig. 1d and Extended Data Fig. 3). LAP-deficient animals also presented with IgG and complement C1q deposition in the glomeruli of kidneys (Fig. 2a–d, Extended Data Fig. 4a, b). In addition, LAP-deficient animals displayed indications of kidney damage[15], and exhibited increased functional markers of kidney injury, such as increased serum creatinine (Fig. 2e), blood urea nitrogen, and proteinuria (Extended Data Fig. 4c, d). Histologically, kidneys from aged LAP-deficient animals displayed endocapillary proliferative glomerulonephritis (Extended Data Fig. 4e). Increased expression of type I interferon (IFN)-regulated genes, termed the IFN signature, has been reported in SLE patients[16]. Analysis revealed increased expression of IFN signature genes, such as *Ddx58* (which encodes RIG-I) and *Isg95* (also known as *Cmtr1*), in the spleens of aged LAP-deficient animals (Extended Data Fig. 5a). By contrast, none of these pathologies was observed in animals lacking autophagy components dispensable for LAP (Fig. 2a–e and Extended Data Figs 4a–e, 5a). Collectively, these observations suggest that LAP deficiency, but not autophagy deficiency, causes an autoinflammatory, lupus-like syndrome in mice.

The kinetics of disease we observed in all LAP-deficient animals was markedly similar to that of animals lacking T-cell immunoglobulin mucin protein 4 (TIM4) (Figs 1a, b and 2a, e). TIM4 is required for engulfment of dying cells in several macrophage populations, and animals lacking TIM4 display lupus-like disease[2], as do animals defective for other proteins involved in the clearance of dying cells, including MERTK, MFG-E8, and C1q (ref. 1). However, we found that neither bone-marrow-derived macrophages (Extended Data Fig. 5b) nor peritoneal exudate macrophages from 52-week-old mice of any genotype (Extended Data Fig. 5c) showed any defects in the engulfment of dying cells *in vitro*. We therefore examined the role of LAP in the response

[1]Department of Immunology, St Jude Children's Research Hospital, Memphis, Tennessee 38105, USA. [2]Immunity, Inflammation, and Disease Laboratory, National Institute of Environmental Health Sciences, 111 T.W. Alexander Drive, Research Triangle Park, North Carolina 27709, USA. [3]Department of Pathology and Immunology, Washington University School of Medicine, St Louis, Missouri 63110, USA. [4]University of Texas Southwestern Medical Center, Dallas, Texas 75390, USA. [5]Division of Nephrology and Hypertension, Christian-Albrechts-University, Kiel 24105, Germany.

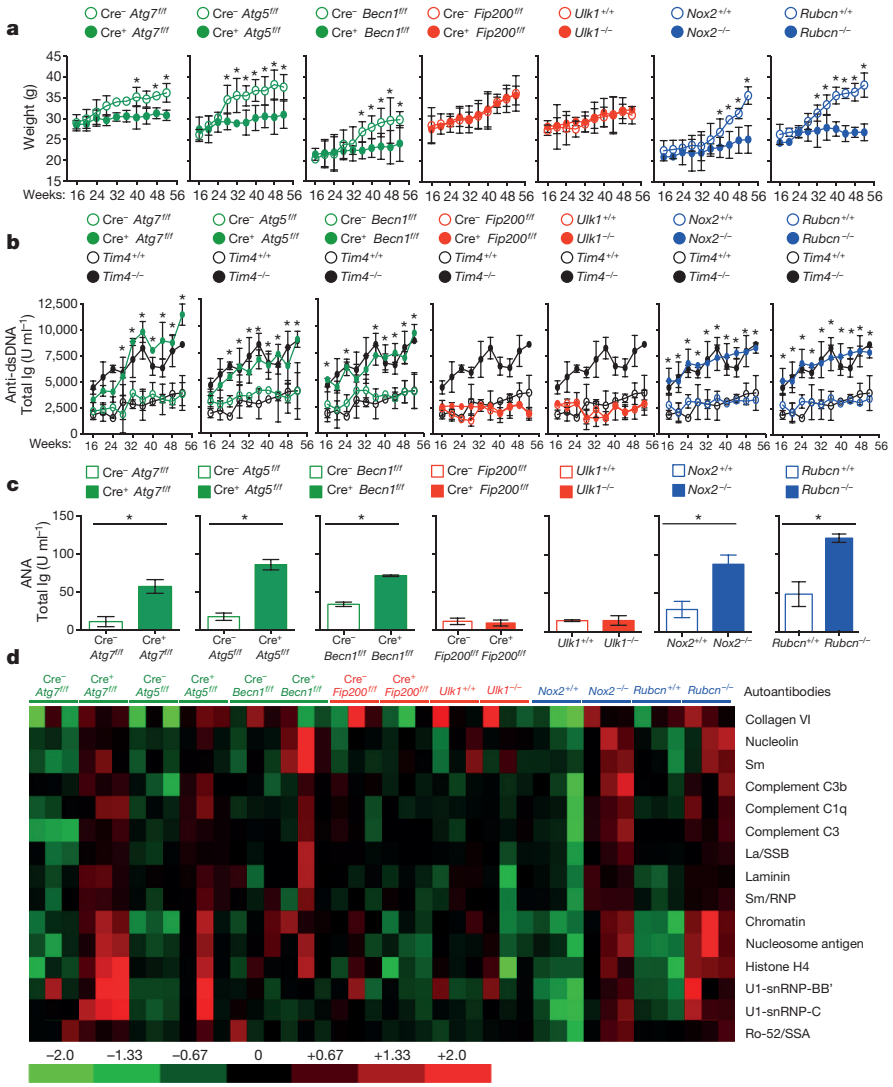

Figure 1 | Mice with LAP deficiencies display symptoms of autoinflammatory disorder. Wild-type and deficient littermates were co-housed and aged for 52 weeks at St Jude Children's Research Hospital (SJCRH). **a**, Weights. **b**, Anti-dsDNA antibodies (total Ig). **c**, **d**, Anti-nuclear antigens (ANA; total Ig) in animals aged 52 weeks (**c**). Antibodies to autoantigens commonly associated with autoimmune and autoinflammatory disorders. Three mice per genotype, normalized background signals (**d**). In all cases, Cre indicates LysM-Cre. Error bars represent s.d. $*P < 0.001$ (Student's *t*-test). Animal numbers are provided in the Methods. Colour scheme represents LAP-deficient, autophagy-deficient genotypes (green), autophagy-deficient, LAP-sufficient (red), and autophagy-sufficient, LAP-deficient (blue). Values for one cohort of $Tim4^{+/+}$ and $Tim4^{-/-}$ animals are shown for comparison in all cases (black) in **a** and **b**.

to dying cells *in vivo*. PKH26-labelled wild-type C57Bl/6 thymocytes were ultraviolet (UV)-irradiated to trigger apoptosis and immediately injected into wild-type animals, or animals with LysM-Cre-mediated deficiency of ATG7 (LAP-deficient, autophagy-deficient), LysM-Cre-mediated deficiency of FIP200 (LAP-sufficient, autophagy-deficient), or ubiquitous deletion of RUBCN (LAP-deficient, autophagy-sufficient), all of which also expressed transgenic green fluorescent protein (GFP)-tagged LC3 (ref. 5). Clearance of dying thymocytes and induction of LC3-II (a measure of LC3 conversion[5]) were monitored in spleen, liver and kidney. While both wild-type and animals with FIP200-deficiency effectively cleared dying cells (Fig. 3a, b and Extended Data Fig. 6a) and converted GFP–LC3 (Extended Data Fig. 6b–d), animals with ATG7- or RUBCN-deficiency did not, despite engulfment (Fig. 3a, b and Extended Data Fig. 6a, b, d, e). These data are consistent with our observations *in vitro*[4], and support the conclusion that LAP is required for effective degradation of engulfed, dying cells *in vivo*. Dying cells were engulfed by $CD11b^+$ $F4/80^+$ macrophages, $CD11b^+$ $Gr1^+$ granulocytes, $CD11b^+$ $CD115^+$ monocytes, and $CD11b^+$ $CD11c^+$ dendritic cells, equivalently in wild-type and $Rubcn^{-/-}$ mice, but not in $Tim4^{-/-}$ (also known as $Timd4^{-/-}$) mice (Extended Data Fig. 6e). However, while the frequency of engulfment declined by 48 h in all cellular subsets in wild-type mice, they remained elevated in $Rubcn^{-/-}$ mice, consistent with a failure of a LAP-dependent mechanism to degrade engulfed corpses (Extended Data Fig. 6e).

Previously, we had found that in contrast to wild-type or $Ulk1^{-/-}$ macrophages, Cre^+ $Atg7^{f/f}$ macrophages produce increased levels of inflammatory cytokines, such as IL-1β and IL-6 *in vitro*[4]. We therefore examined cytokine production after ingestion of dying cells in macrophages lacking different components of the LAP or autophagy pathways (Extended Data Fig. 7a–d). LAP-deficient (Cre^+ $Atg7^{f/f}$, Cre^+ $Becn1^{f/f}$, Cre^+ $Atg3^{f/f}$, $Nox2^{-/-}$ (also known as $Cybb^{-/-}$) and $Rubcn^{-/-}$; Cre indicates LysM-Cre throughout) but not LAP-sufficient (Cre^+ $Fip200^{f/f}$, Cre^+ $Atg14^{f/f}$) macrophages produced IL-1β, IL-6 and IP-10 (also known as CXCL10), upon engulfment of dying cells (Extended Data Fig. 7a–c). Conversely, LAP-sufficient, but not LAP-deficient macrophages produced IL-10 upon engulfment (Extended Data Fig. 7d). We then examined the effects of dying cells on serum cytokine production *in vivo*, after injection of UV-irradiated thymocytes (Fig. 3c, d). Notably, serum IL-1β, IL-6 and MIP-1β (also known as CCL4) were acutely increased in LAP-deficient animals (ATG7 or RUBCN), but not in LAP-sufficient animals (wild-type or FIP200) (Fig. 3c, d). As observed *in vitro*, LAP-sufficient animals produced increased serum IL-10 in response to dying cells, whereas LAP-deficient animals did not (Fig. 3c, d). Therefore, LAP, but not canonical autophagy, is required for the production of IL-10 in response to apoptotic cell engulfment, and LAP suppresses the production of inflammatory cytokines under these conditions.

We next asked whether repeated injection of apoptotic thymocytes into LAP-deficient animals could exacerbate the SLE-like phenotype observed in aged LAP-deficient animals. Beginning at 6 weeks of age, $Rubcn^{+/+}$ and $Rubcn^{-/-}$ animals were injected with UV-irradiated thymocytes over an 8-week period. Uninjected $Rubcn^{+/+}$ animals showed a minimal

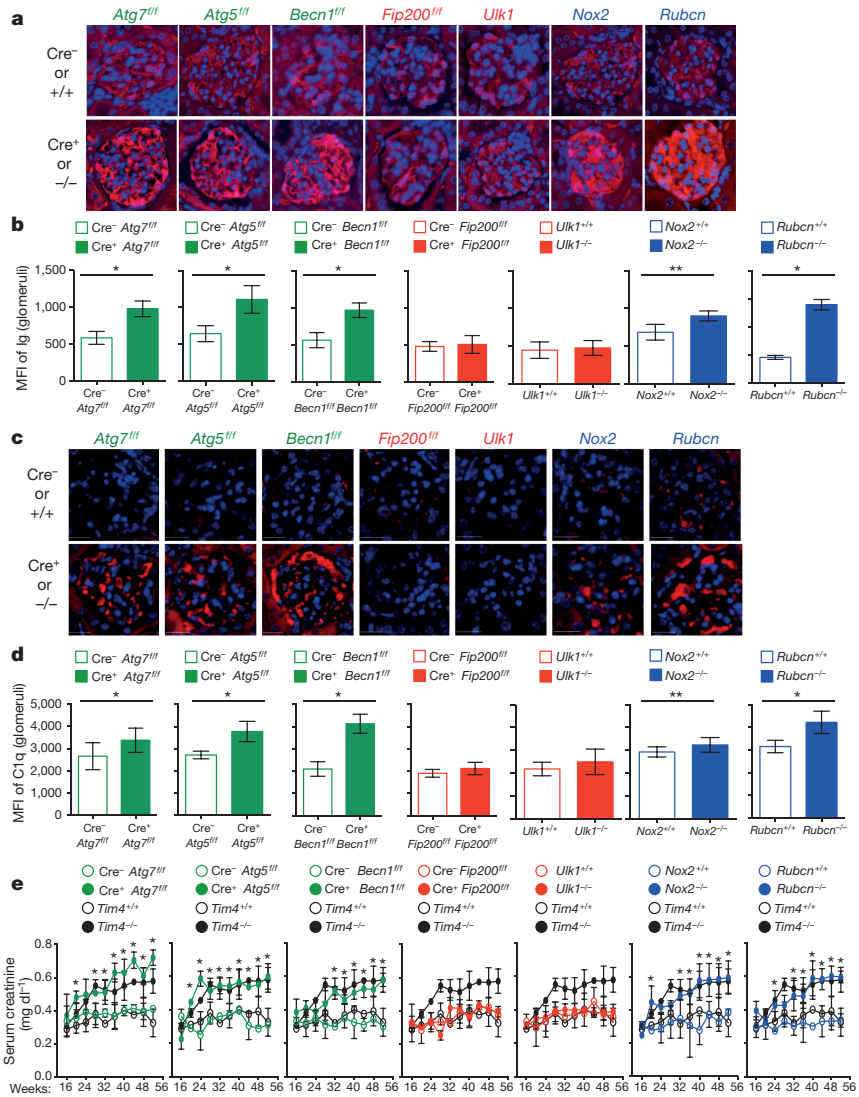

Figure 2 | Mice with LAP deficiencies display kidney pathology. a–d, Appearance of kidneys of co-housed, 52-week-old animals. DAPI (blue), anti-IgG (red, **a**), anti-C1q (red, **c**). Original magnifications, ×100. Mean fluorescent intensity (MFI) of anti-IgG (**b**) and anti-C1q (**d**) in glomeruli. **e**, Serum creatinine. Animal numbers are provided in Methods. Error bars represent s.d. ($*P < 0.001$, $**P < 0.05$, Student's *t* test). For histological assessment, at least 15 glomeruli were evaluated for each genotype. Colour scheme represents LAP-deficient, autophagy-deficient genotypes (green), autophagy-deficient, LAP-sufficient (red), and autophagy-sufficient, LAP-deficient (blue). Values for one cohort of $Tim4^{+/+}$ and $Tim4^{-/-}$ animals are shown for comparison in all cases (black) in **e**.

increase in anti-nuclear antigens (ANA) and anti-dsDNA autoantibodies after 8 weeks, and no increase attributable to injection of dying cells. $Rubcn^{-/-}$ animals, however, displayed a significant increase in serum levels of ANA and anti-dsDNA autoantibodies after 8 weeks of dying cell injections, above pre-injection and age-matched, uninjected controls (Fig. 3e). Furthermore, these animals displayed IgG and C1q deposition in the glomeruli of kidneys (Extended Data Fig. 8a, b), and injected $Rubcn^{-/-}$ animals displayed increased levels of alanine aminotransferase, indicative of tissue damage (Extended Data Fig. 8c). Collectively, these data demonstrate that defective dead cell clearance associated with LAP deficiency can result in development of SLE-like disease.

We next examined spontaneous levels of serum cytokines with age in animals with or without LAP. All genotypes lacking LAP (Cre^{+} $Atg7^{f/f}$, Cre^{+} $Atg5^{f/f}$, Cre^{+} $Becn1^{f/f}$, $Nox2^{-/-}$ and $Rubcn^{-/-}$) displayed increased levels of IL-1β, IL-6, IL-12p40 and IP-10 (Fig. 4a–d), as well as KC (also known as CXCL1), MIP-1β and MCP-1 (also known as CCL2) (Extended Data Fig. 8d–f). Wild-type animals and animals lacking canonical autophagy, but not LAP (in monocytes or systemically), did not display increased inflammatory cytokines at any time point (Fig. 4a–d and Extended Data Fig. 8d–f). By contrast, serum IL-10 levels, which increased with age in LAP-sufficient strains, were undetectable in animals lacking LAP (Fig. 4e). The patterns and kinetics of cytokine levels were similar to that observed in $Tim4^{-/-}$ animals (Fig. 4a–e and Extended Data Fig. 8d–f).

Our observations indicated that defects in LAP, but not canonical autophagy, cause an autoinflammatory, lupus-like syndrome in mice. To test this idea further, we examined both LAP-sufficient and LAP-deficient mice bred in an independent facility. Mice with ATG5- or ATG3-deficient myeloid cells (defective in LAP and autophagy) displayed increased levels of IL-1β, IL-6, IL-12p40, IP-10, KC, MIP-1β and MCP-1 at 52 weeks of age (Extended Data Fig. 9a–g). These LAP-deficient animals also displayed significantly lower levels of IL-10 than controls (Extended Data Fig. 9h). Furthermore, LAP-deficient animals displayed elevated anti-dsDNA antibodies (Extended Data Fig. 9i) and serum creatinine (Extended Data Fig. 9J). LAP-deficient animals also contained a broad array of antibodies against autoantigens commonly associated with SLE (Extended Data Fig. 10). Of note, none of these effects was observed in animals with ATG14- or FIP200-deficiency (defective autophagy but normal LAP[3,6,7,11,13]) (Extended Data Figs 9a–j, 10). It is noteworthy that these effects in two different facilities were observed in C57Bl/6 background animals, which are generally resistant to lupus-like disease[17]. Previous studies have shown that one of the LAP-deficient genotypes, $Nox2^{-/-}$, causes accelerated, severe lupus-like disease when bred on the lupus-prone MRL.lpr background[18].

Altogether, these data suggest that defective LAP results in a failure to digest engulfed dying cells, leading to increased inflammatory cytokine production and a lupus-like syndrome. In another study, animals in which lung macrophages were incapable of engulfment owing to deletion of RAC1 were sensitive to inflammatory cytokine production and inflammatory disease after introduction of dying cells into the lung[19]. Similarly, TIM4-deficient mice, which exhibit defective dead cell

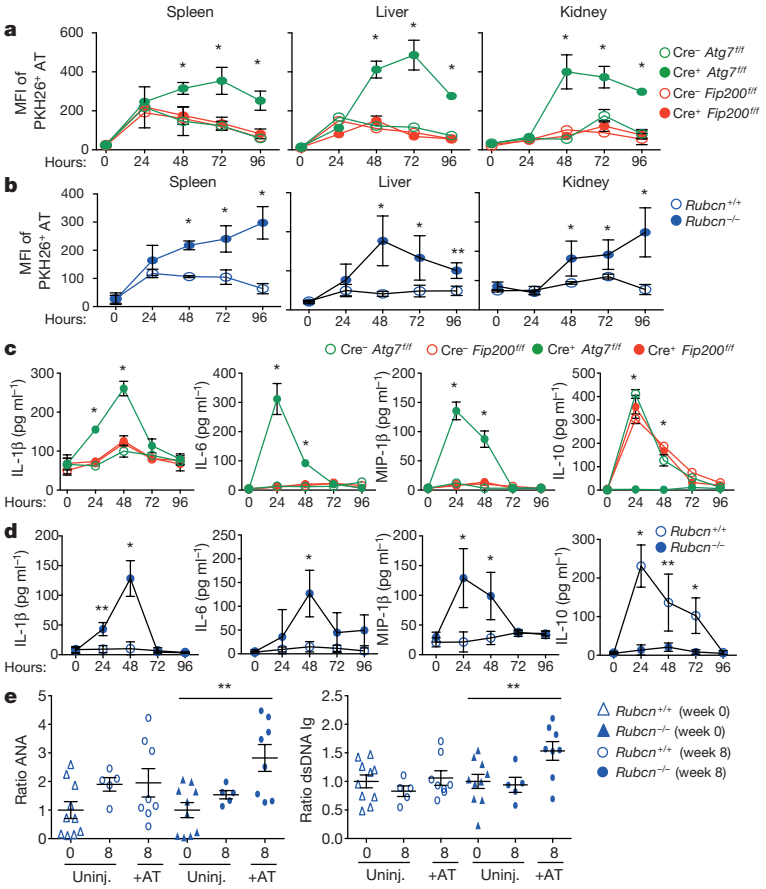

Figure 3 | Mice with LAP deficiencies display defective clearance of engulfed, dying cells, resulting in increased production of pro-inflammatory cytokines. a–d, 1×10^7 PKH26-labelled UV-irradiated wild-type thymocytes were injected intravenously into indicated animals expressing GFP–LC3. Apoptotic thymocytes (AT) in spleen, liver and kidney of indicated animals measured by flow cytometry (**a**, **b**). Indicated serum cytokines (**c**, **d**). Error bars represent s.d. ($n = 4$, $^*P < 0.001$, $^{**}P < 0.05$, Student's t-test). **e**, 2×10^7 UV-irradiated wild-type thymocytes were injected intravenously six times over 8 weeks into indicated animals (aged 6 weeks). Serum anti-nuclear antibodies (total Ig) and anti-dsDNA antibodies (total Ig) are shown at 16 weeks from uninjected (uninj.) and injected (+AT) animals. Results are presented as ratio to average value before injection for each individual animal. Error bars represent s.e.m. ($n = 4$, $^{**}P < 0.05$, Student's t-test). The colour scheme represents LAP-deficient, autophagy-deficient genotypes (green), autophagy-deficient, LAP-sufficient (red), and autophagy-sufficient, LAP-deficient (blue).

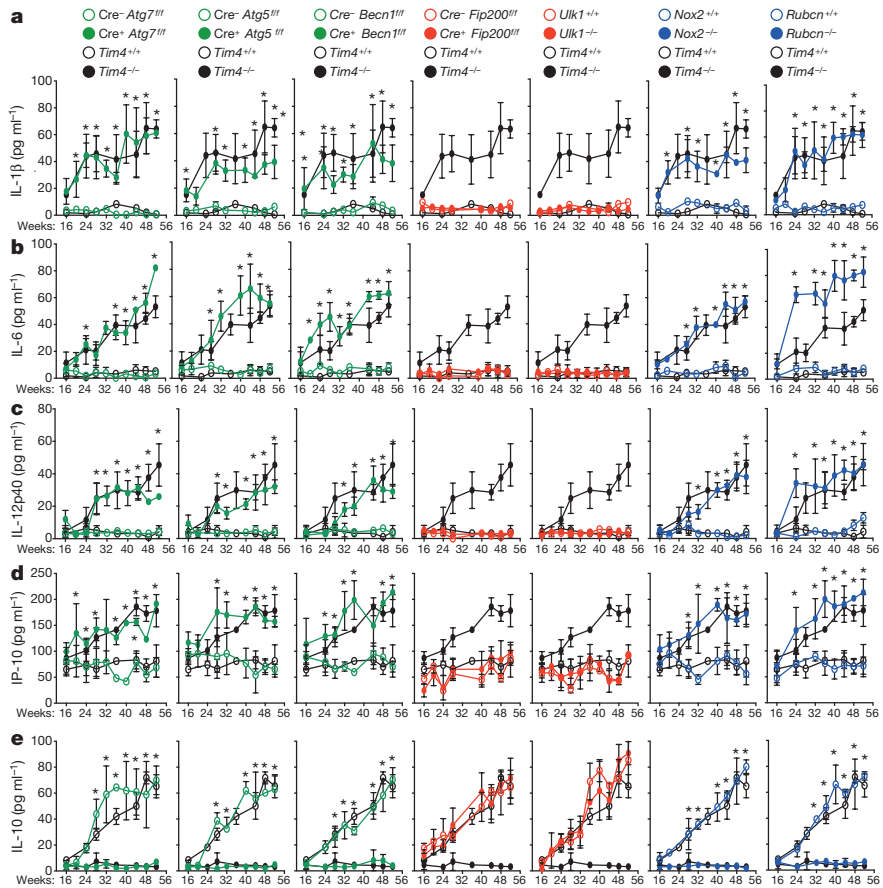

Figure 4 | Mice with LAP deficiencies display symptoms of an autoinflammatory disorder. a–e, Indicated serum cytokines in co-housed 52-week-old animals. Error bars represent s.d. ($^*P < 0.001$, Student's t-test). Numbers of animals are provided in Methods. Colour scheme represents LAP-deficient, autophagy-deficient genotypes (green), autophagy-deficient, LAP-sufficient (red), and autophagy-sufficient, LAP-deficient (blue). Values for one cohort of $Tim4^{+/+}$ and $Tim4^{-/-}$ animals are shown for comparison in all cases (black) in **a–e**.

engulfment[2], showed spontaneous increases in serum inflammatory cytokines with age (Fig. 4 and Extended Data Fig. 8) as well as lupus-like disease (Figs 1 and 2). By contrast, macrophages defective for LAP engulf dying cells, but fail to digest them efficiently[4,7]. This suggests that LAP-dependent digestion of dying cells, rather than engulfment alone, suppresses an inflammatory response by macrophages. In the absence of LAP (lack of BECN1, ATG7, ATG5, NOX2, RUBCN), macrophages engulf dying cells and produce inflammatory cytokines, and animals manifest lupus-like disease. However, when canonical autophagy, but not LAP, is defective (lack of FIP200, ULK1), dying cells are engulfed, macrophages produce IL-10 but not inflammatory cytokines, and no lupus-like disease is observed.

MRL.lpr mice lacking IL-10 display markedly accelerated lupus-like disease[20]. While macrophages, monocytes and B cells are the major source of IL-10, specific deletion of IL-10 in B cells had no effect on pathogenesis in MRL.lpr mice[21]. Notably, one study found that injection of dendritic cells that had engulfed necrotic cells into IL-10-deficient, but not wild-type mice induced a pronounced lupus-like disease[22]. Thus, the role of LAP in the production of IL-10 may contribute to the disease effects we observed. However, most studies have implicated increased IL-10 levels in mouse and human SLE[20,23,24], perhaps involved with the activation of B lymphocytes[25]. While IL-10 production in response to dying cells was compromised in LAP-deficient macrophages, the production of IL-10 in response to other stimuli may remain intact, and thus increased IL-10 in SLE may be due to other events in the pathogenesis of SLE.

Genome-wide association studies have implicated autophagy in SLE (*Atg5* (refs 6, 8) and possibly *Atg7* (ref. 9)) and in Crohn's disease (*Atg16l*; ref. 26). It is notable in this context that the ATG5 association with SLE may depend on polymorphisms in IL-10 (refs 8, 27). Other studies have suggested that autophagy suppresses the inflammasome[28], providing a possible link between autophagy and inflammatory disease. However, the autophagic components identified in these studies are also required for LAP. Furthermore, mice[18] and humans[29] lacking NOX2 develop SLE, and our studies suggest that defective LAP in this context may contribute to this effect. Our findings implicate a non-canonical autophagic process, LAP, in the control of inflammatory disease and suggest a link between the clearance of dying cells, autophagic processes, and inflammation in the control of SLE.

Online Content Methods, along with any additional Extended Data display items and Source Data, are available in the online version of the paper; references unique to these sections appear only in the online paper.

Received 6 March 2015; accepted 1 April 2016.
Published online 20 April 2016.

1. Ravichandran, K. S. Find-me and eat-me signals in apoptotic cell clearance: progress and conundrums. *J. Exp. Med.* **207,** 1807–1817 (2010).
2. Rodriguez-Manzanet, R. *et al.* T and B cell hyperactivity and autoimmunity associated with niche-specific defects in apoptotic body clearance in TIM-4-deficient mice. *Proc. Natl Acad. Sci. USA* **107,** 8706–8711 (2010).
3. Kim, J. Y. *et al.* Noncanonical autophagy promotes the visual cycle. *Cell* **154,** 365–376 (2013).
4. Martinez, J. *et al.* Microtubule-associated protein 1 light chain 3 α (LC3)-associated phagocytosis is required for the efficient clearance of dead cells. *Proc. Natl Acad. Sci. USA* **108,** 17396–17401 (2011).
5. Martinez, J. *et al.* Molecular characterization of LC3-associated phagocytosis (LAP) reveals distinct roles for Rubicon, NOX2, and autophagy proteins. *Nature Cell Biol.* **17,** 893–906 (2015).
6. Henault, J. *et al.* Noncanonical autophagy is required for type I interferon secretion in response to DNA-immune complexes. *Immunity* **37,** 986–997 (2012).
7. Florey, O., Kim, S. E., Sandoval, C. P., Haynes, C. M. & Overholtzer, M. Autophagy machinery mediates macroendocytic processing and entotic cell death by targeting single membranes. *Nature Cell Biol.* **13,** 1335–1343 (2011).
8. Zhou, X. J. *et al.* Genetic association of PRDM1–ATG5 intergenic region and autophagy with systemic lupus erythematosus in a Chinese population. *Ann. Rheum. Dis.* **70,** 1330–1337 (2011).
9. Clarke, A. J. *et al.* Autophagy is activated in systemic lupus erythematosus and required for plasmablast development. *Ann. Rheum. Dis.* **74,** 912–920 (2015).
10. Sanjuan, M. A. *et al.* Toll-like receptor signalling in macrophages links the autophagy pathway to phagocytosis. *Nature* **450,** 1253–1257 (2007).
11. Gan, B. & Guan, J. L. FIP200, a key signaling node to coordinately regulate various cellular processes. *Cell. Signal.* **20,** 787–794 (2008).
12. Mizushima, N. & Levine, B. Autophagy in mammalian development and differentiation. *Nature Cell Biol.* **12,** 823–830 (2010).
13. Matsunaga, K. *et al.* Two Beclin 1-binding proteins, Atg14L and Rubicon, reciprocally regulate autophagy at different stages. *Nature Cell Biol.* **11,** 385–396 (2009).
14. Clausen, B. E., Burkhardt, C., Reith, W., Renkawitz, R. & Forster, I. Conditional gene targeting in macrophages and granulocytes using LysMcre mice. *Transgenic Res.* **8,** 265–277 (1999).
15. Theofilopoulos, A. N. & Dixon, F. J. Murine models of systemic lupus erythematosus. *Adv. Immunol.* **37,** 269–390 (1985).
16. Rönnblom, L. & Eloranta, M. L. The interferon signature in autoimmune diseases. *Curr. Opin. Rheumatol.* **25,** 248–253 (2013).
17. Morel, L., Rudofsky, U. H., Longmate, J. A., Schiffenbauer, J. & Wakeland, E. K. Polygenic control of susceptibility to murine systemic lupus erythematosus. *Immunity* **1,** 219–229 (1994).
18. Campbell, A. M., Kashgarian, M. & Shlomchik, M. J. NADPH oxidase inhibits the pathogenesis of systemic lupus erythematosus. *Sci. Transl. Med.* **4,** 157ra141 (2012).
19. Juncadella, I. J. *et al.* Apoptotic cell clearance by bronchial epithelial cells critically influences airway inflammation. *Nature* **493,** 547–551 (2013).
20. Yin, Z. *et al.* IL-10 regulates murine lupus. *J. Immunol.* **169,** 2148–2155 (2002).
21. Teichmann, L. L. *et al.* B cell-derived IL-10 does not regulate spontaneous systemic autoimmunity in MRL.*Fas*^{lpr} mice. *J. Immunol.* **188,** 678–685 (2012).
22. Ma, L. *et al.* Systemic autoimmune disease induced by dendritic cells that have captured necrotic but not apoptotic cells in susceptible mouse strains. *Eur. J. Immunol.* **35,** 3364–3375 (2005).
23. Perry, D., Sang, A., Yin, Y., Zheng, Y. Y. & Morel, L. Murine models of systemic lupus erythematosus. *J. Biomed. Biotechnol.* **2011,** 271694 (2011).
24. Houssiau, F. A. *et al.* Serum interleukin 10 titers in systemic lupus erythematosus reflect disease activity. *Lupus* **4,** 393–395 (1995).
25. Blenman, K. R. *et al.* IL-10 regulation of lupus in the NZM2410 murine model. *Lab. Invest.* **86,** 1136–1148 (2006).
26. Hampe, J. *et al.* A genome-wide association scan of nonsynonymous SNPs identifies a susceptibility variant for Crohn disease in *ATG16L1*. *Nature Genet.* **39,** 207–211 (2007).
27. López, P., Alonso-Pérez, E., Rodriguez-Carrio, J. & Suárez, A. Influence of Atg5 mutation in SLE depends on functional IL-10 genotype. *PLoS ONE* **8,** e78756 (2013).
28. Shi, C. S. *et al.* Activation of autophagy by inflammatory signals limits IL-1beta production by targeting ubiquitinated inflammasomes for destruction. *Nature Immunol.* **13,** 255–263 (2012).
29. De Ravin, S. S. *et al.* Chronic granulomatous disease as a risk factor for autoimmune disease. *J. Allergy Clin. Immunol.* **122,** 1097–1103 (2008).

Supplementary Information is available in the online version of the paper.

Acknowledgements The authors thank T. Brewer, P. Fitzgerald, J. Kolb and T. Oguin for technical assistance. We also thank K. Gerrish and R. Fannin for their work and analysis of the Nanostring data. This work was supported by the Intramural Research Program of the National Institutes of Health, NIEHS (1ZIAES10328601), as well as grants from the US National Institutes of Health (RO1 AI40646, U19 AI109725), the Lupus Research Institute, the German Research Foundation (EXC306), and ALSAC.

Author Contributions J.M. and D.R.G. designed the experiments; J.M. performed and analysed the experiments; L.D.C., S.P., M.Y., Q.L., Q.-Z.L., M.Y., L.J., C.G., A.L. and R.O. performed and analysed specific experiments; J.M., H.W.V. and D.R.G. wrote the manuscript.

Author Information Reprints and permissions information is available at www.nature.com/reprints. The authors declare no competing financial interests. Readers are welcome to comment on the online version of the paper. Correspondence and requests for materials should be addressed to D.R.G. (douglas.green@stjude.org) or J.M. (jennifer.martinez3@nih.gov).

METHODS

Mice and primary cells. All mice were housed specific pathogen-free.

Ulk1$^{-/-}$ mice were provided by M. Kundu. *Atg7*$^{f/f}$ mice (provided by M. Komatsu) were bred to LysM-Cre^{+} mice (provided by P. Murray) and GFP-LC3^{+} mice to generate LysM-Cre^{+} *Atg7*$^{f/f}$ GFP–LC3^{+} versions of these strains. *Nox2*$^{-/-}$ mice were purchased from Jackson Laboratories. LysM-Cre^{+} *Becn1*$^{f/f}$ (E. Rucker), LysM-Cre^{+} *Atg5*$^{f/f}$ (T. A. Ferguson), and LysM-Cre^{+} *Fip200*$^{f/f}$ (J.-L. Guan) were bred to GFP-LC3^{+} mice to generate GFP–LC3^{+} versions of these strains. *Tim4*$^{-/-}$ mice were provided by V. Kuchroo. *Rubcn*$^{+/+}$ and *Rubcn*$^{-/-}$ mice were generated using CRISPR/Cas9 gene editing technology[5]. LysM-Cre^{+} *Atg14*$^{f/f}$, LysM-Cre^{+} *Atg3*$^{f/f}$, LysM-Cre^{+} *Atg5*$^{f/f}$, LysM-Cre^{+} *Fip200*$^{f/f}$ mice (and control littermates) were bred and maintained in the Washington University facility. The St Jude Institutional Animal Care and Use Committee approved all procedures in accordance with the Guide for the Care and Use of Animals.

Bone-marrow-derived macrophages were generated from bone marrow progenitors obtained from littermates. Freshly prepared bone marrow cells were cultured in DMEM medium supplemented with 10% heat-inactivated FCS, 2 mM L-glutamine, 10 mM HEPES buffer, 50 μg ml^{-1} penicillin, and non-essential amino acids in the presence of 20 ng ml^{-1} rmM-CSF (Peprotech) for 6 days. Nonadherent cells were removed on day 6, and adherent macrophages were detached from plates and re-plated for experimental use.

Ageing studies. Male wild-type and knockout littermates were co-housed and allowed to age for 52 weeks. Animals were weighed and bled retro-orbitally monthly, and serum was collected for use in assays (below). Numbers of animals were as follows (in all cases, Cre indicates LysM-Cre). Studies conducted at St Jude Children's Research Hospital and reported in Figs 1, 2, 4 and Extended Data Figs 2–5 and 8: Cre^{-} and Cre^{+} *Atg7*$^{f/f}$, $n = 24$ per genotype; Cre^{-} and Cre^{+} *Atg5*$^{f/f}$, $n = 14$ per genotype; Cre^{-} and Cre^{+} *Becn1*$^{f/f}$, $n = 20$ per genotype; Cre^{-} and Cre^{+} *Fip200*$^{f/f}$, $n = 16$ per genotype; *Ulk1*$^{+/+}$ and *Ulk1*$^{-/-}$, $n = 14$ per genotype; *Nox2*$^{+/+}$ and *Nox2*$^{-/-}$, $n = 10$ per genotype; *Rubcn*$^{+/+}$ and *Rubcn*$^{-/-}$, $n = 14$ per genotype. Studies conducted at Washington University and reported in Extended Data Figs 9 and 10: Cre^{-} and Cre^{+} *Atg5*$^{f/f}$, $n = 5$ per genotype; Cre^{-} and Cre^{+} *Atg3*$^{f/f}$, $n = 4$ per genotype; Cre^{-} and Cre^{+} *Fip200*$^{f/f}$, $n = 4$ per genotype; Cre^{-} and Cre^{+} *Atg14*$^{f/f}$, $n = 4$ per genotype.

Induction of apoptosis in thymocytes. Apoptosis was induced in wild-type C57Bl/6 thymocytes by UV irradiation (20 J m^{-2}). Thymocytes were washed twice with PBS before experimental use.

Staining of apoptotic thymocytes and *in vivo* adoptive transfer of labelled apoptotic thymocytes. UV-treated thymocytes were stained with 20 M PKH26 Red (Sigma), per manufacturer's instructions. 1×10^7 PKH26-labelled, apoptotic thymocytes were injected intravenously into GFP–LC3^{+} animals, and serum, kidney, liver and spleen was collected at 0, 24, 48, 72 and 96 h after injection. Kidney sections were analysed for persistence of PKH26-labelled apoptotic cells using the Nikon800 microscope. Kidney, liver and spleen samples were analysed for PKH26-labelled apoptotic cells using flow cytometry. Additionally, samples were washed once with FACS buffer and permeabilized with digitonin (Sigma, 200 μg ml^{-1}) for 15 min on ice. Cells were then washed three times with FACS buffer and analysed by flow cytometry for membrane-bound GFP–LC3-II associated with engulfed PKH26-labelled thymocytes. For quantification of phagocytosis, spleens were harvested and stained for fluorescently conjugated surface markers for macrophages (CD11b^{+} F4/80^{+}), neutrophils (CD11b^{+} Gr-1^{+}), monocytes (CD11b^{+} CD115^{+}), and dendritic cells (CD11b^{+} CD11c^{+}). Phagocytic efficiency of each cell type (singlets/cell surface markers^{+}/PKH26^{+}) was quantified by flow cytometry (percentage PKH26).

Repeated injection of apoptotic thymocytes. Six-week-old *Rubcn*$^{+/+}$ and *Rubcn*$^{-/-}$ littermates were used. Serum was collected from all animals before injection (week 0). 2.0×10^7 UV-irradiated thymocytes (20 J m^{-2}) suspended in sterile phosphate buffer were injected intravenously (i.v.) into anaesthesized mice, once a week for four consecutive weeks (from weeks 1 to 4). After a resting period of 15 days, the injections were resumed and carried out for other 2 weeks (weeks 6 and 7). Serum was collected 1 week after the last injection (week 8) and assessed for levels of anti-dsDNA autoantibodies (total Ig), ANA (total Ig), and alanine aminotransferase. At week 8, mice were euthanized, the kidneys were collected and stained for immunofluorescence (below).

Collection and co-culture of peritoneal exudate cells. For collection of peritoneal exudate cells, mice were injected intraperitoneally (i.p.) with 2 ml of 3% Brewer's thioglycollate and euthanized 96 h later. The peritoneum was washed with 10 ml ice-cold PBS three times. Cells were centrifuged (225*g*, 6 min, 4 °C) and washed twice with sterile PBS. Peritoneal exudate cells were resuspended in DMEM plus 10% FBS, counted and plated at 5×10^5 cells per well in a 12-well plate. Cells were allowed to settle for 2 h (37 °C, 5% CO_2) before co-culture with UV-irradiated wild-type thymocytes.

Effects of dying cells on macrophages *in vitro*. Apoptotic thymocytes were added to BMDM cultures at a ratio of 10:1 (dead cell:macrophage). Supernatant was collected after 24 h of culture and analysed for cytokines (see below).

Flow cytometry analysis. Spleens, livers and kidneys were collected from animals at the indicated time points, and single-cell suspensions were generated. Cells were washed once with FACS buffer, and permeabilized with digitonin (Sigma, 200 μg ml^{-1}) for 15 min on ice. Cells were then washed three times with FACS buffer and analysed by flow cytometry for membrane-bound GFP–LC3-II. This assay removes the soluble, cytosolic form of GFP–LC3 (GFP–LC3-I), while the lipidated, membrane-bound GFP–LC3-II is retained, allowing total GFP fluorescence to be used as a measure of LC3-II generation, indicative of LAP. Permeabilized samples were first gated on singlets/PKH26^{+}, so as to determine the MFI of GFP–LC3-II associated with cells that had engulfed a PKH26^{+} apoptotic thymocyte. For surface staining, blood, bone marrow or splenocytes were washed once with FACS buffer, incubated with Fc Block and stained with the indicated fluorescent antibodies (Biolegend) on ice for 20 min. Cells were then washed twice with FACS buffer and analysed by flow cytometry. Data were acquired using an LSRII cytometer (BD).

Quantification of phagocytosis. Phagocytosis was quantified using flow cytometry analysis (described above). Apoptotic thymocytes were stained with CellTrace Violet (Molecular Probes) or PKH26 (Sigma-Aldrich) per manufacturer's protocol. Percentage phagocytosis equals the percentage of cells that have engulfed CellTrace Violet^{+} or PKH26^{+} apoptotic thymocytes.

Immunofluorescent staining and analysis of IgG and C1q deposition in kidney sections. Kidneys were collected from animals at 32, 52 or 8 weeks after chronic apoptotic thymocyte injection (above). Organs were sectioned and mounted on slides. Slides were fixed with 4% formaldehyde for 20 min at 4 °C. Following fixation, slides were blocked and permeabilized in block buffer (1% BSA, 0.1% Triton in PBS) for 1 h at room temperature. Slides were washed extensively in TBS containing 0.05% Tween-20 (TBS-Tween), incubated with Alexa-Fluor 647-conjugated anti-IgG (Invitrogen) for 1 h at room temperature, and mounted with VectaShield with DAPI (Vector Labs). Alternatively, slides were washed extensively in TBS-Tween, incubated with anti-C1q (clone 4.8, Abcam) for 1 h at room temperature, washed again with TBS-Tween, incubated with Cy3-conjugated donkey anti-rabbit IgG (Jackson ImmunoResearch) and Alexa-Fluor 488-conjugated wheat germ agglutinin (Molecular Probes) for 1 h at room temperature, and mounted with VectaShield with DAPI (Vector Labs). Images were analysed using an Olympus BX51 FL Microscope and Slidebook software. Masks were drawn around glomeruli, and the MFI values of anti-IgG or anti-C1q were calculated.

Cytokine detection. Supernatants were collected from macrophages fed with apoptotic thymocytes for 24 h. Cytokines released into supernatant were analysed by Luminex technologies (Millipore). Serum was collected from animals was analysed by Luminex technologies (Millipore).

Detection of serum creatinine. The Veterinary Pathology Core at St Jude Children's Research Hospital measured serum creatinine.

Blood and urine clinical chemistry. The Veterinary Pathology Core at St Jude Children's Research Hospital assessed differential blood counts, alanine aminotransferase, and proteinuria (albumin to creatinine ratio). The Clinical Pathology Core at the National Institute of Environmental Health Sciences performed blood urea nitrogen analysis.

Assessment of endocapillary proliferative glomerulonephritis. Kidneys were collected from 52-week-old mice. Organs were sectioned, fixed in 10% formalin, and embedded in paraffin. Four to six micrometre serial sections were cut, deparaffinized, rehydrated and stained with haematoxylin and eosin. All slides were coded before evaluation, and only decoded upon collection of all data. Endocapillary proliferative glomerulonephritis, a glomerular disease pattern frequently associated with lupus nephritis, was assessed on a virtual scale ranging from 0 to 5, where '0' was considered 'indistinguishable compared to wild type control' and '5' was considered 'the maximal damage seen in all samples', based on the classification of glomerulonephritis in systemic lupus erythematosus. Features that influence this score are intraglomerular mesangial proliferation in relation to overall glomerular size, number of mesangial nuclei, intraluminal diameters of glomerular capillaries and the amount of mesangial matrix. Haematoxylin-and-eosin-stained sections were used to score at least 24 glomeruli in a maximum of 4 different specimens obtained from each group.

Detection of anti-dsDNA antibodies and ANA. The presence of anti-dsDNA antibodies in serum was tested using Mouse Anti-dsDNA Igs (Total A+G+M) ELISA Kit (Alpha Diagnostics International), per manufacturer's protocol. The presence of ANA in serum was tested using Mouse ANA/ENA Igs (Total A+G+M) ELISA Kit (Alpha Diagnostics International), per manufacturer's protocol.

Detection of circulating autoantigen using autoantigen microarray. Autoantibody reactivities against a penal of 124 autoantigens were measured

using an autoantigen microarray platform developed by University of Texas Southwestern Medical (https://microarray.swmed.edu/products/category/protein-array/). In brief, serum samples were pretreated with DNase-I and then diluted 1:50 in PBS plus 0.05% Tween-20 buffer for autoantibody profiling. The autoantigen array bearing 124 autoantigens and 4 control proteins were printed in duplicates onto Nitrocellulose film slides (Grace Bio-Labs). The diluted serum samples were incubated with the autoantigen arrays, and autoantibodies were detected with Cy3-labelled anti-mouse IgG and Cy5-labelled anti-mouse IgM using a Genepix 4200A scanner (Molecular Device) with laser wavelength of 532 nm and 635 nm. The resulting images were analysed using Genepix Pro 6.0 software (Molecular Devices). The median of the signal intensity for each spot was calculated and subtracted the local background around the spot, and data obtained from duplicate spots were averaged. The background subtracted signal intensity of each antigen was normalized to the average intensity of the total mouse IgG, which was included on the array as an internal control. Finally, the net fluorescence intensity for each antigen was calculated by subtracting a PBS control that was included for each experiment as negative control. The signal-to-noise ratio was used as a quantitative measurement of the true signal above background noise. Signal-to-noise ratio values equal to or greater than 3 were considered significantly higher than background, and therefore true signals. The net fluorescence intensity of each autoantibody was used to generate heatmaps using Cluster and Treeview software (http://bonsai.hgc.jp/~mdehoon/software/cluster/software.htm). Each row in the heatmap represents an autoantibody, and each column represents a sample. Red colour represents the signal intensity higher than the mean value of the raw, and green colour means signal intensity is lower than the mean value of the raw.

RNA extraction and nanostring analysis. Total RNA was isolated from the spleens from 52-week-old mice using NucleoSpin II kit (Macherey-Nagel) according to the manufacturer's instructions, and 50 ng was used to determine the absolute levels of gene expression. Hybridization and nCounter were performed according to the manufacturer's protocol (Nanostring Technologies). In brief, reactions were hybridized for 20 h at 65 °C, after which the products were used to run on the nCounter preparation station for removal of excess probes. Data were collected with the nCounter digital analyser by counting individual barcodes. Data generated from the nCounter digital analyser were examined with the nCounter digital analyser software system v2.1.1 (Nanostring Technologies). Data were normalized to the geometric means of spiked-in positive controls (controls for assay efficiency) and spiked-in negative controls (normalized for background). The data were further normalized to the housekeeping genes *Gapdh*, *Hprt* and *Tubb5* and are reported as normalized RNA counts (means ± s.e.m.). Nanostring RNA counts were analysed with the Partek Genomic Suite, to identify significantly regulated probe. Heatmaps of Nanostring data were generated with the Partek Genomic Suite.

Statistical analysis. The statistical significance of differences in mean values was calculated using unpaired, two-tailed Student's *t*-test. *P* values less than 0.05 were considered statistically significant. No statistical methods were used to predetermine sample size. Experiments were not randomized, and the investigators were not blinded to allocation during experiments and outcome assessment.

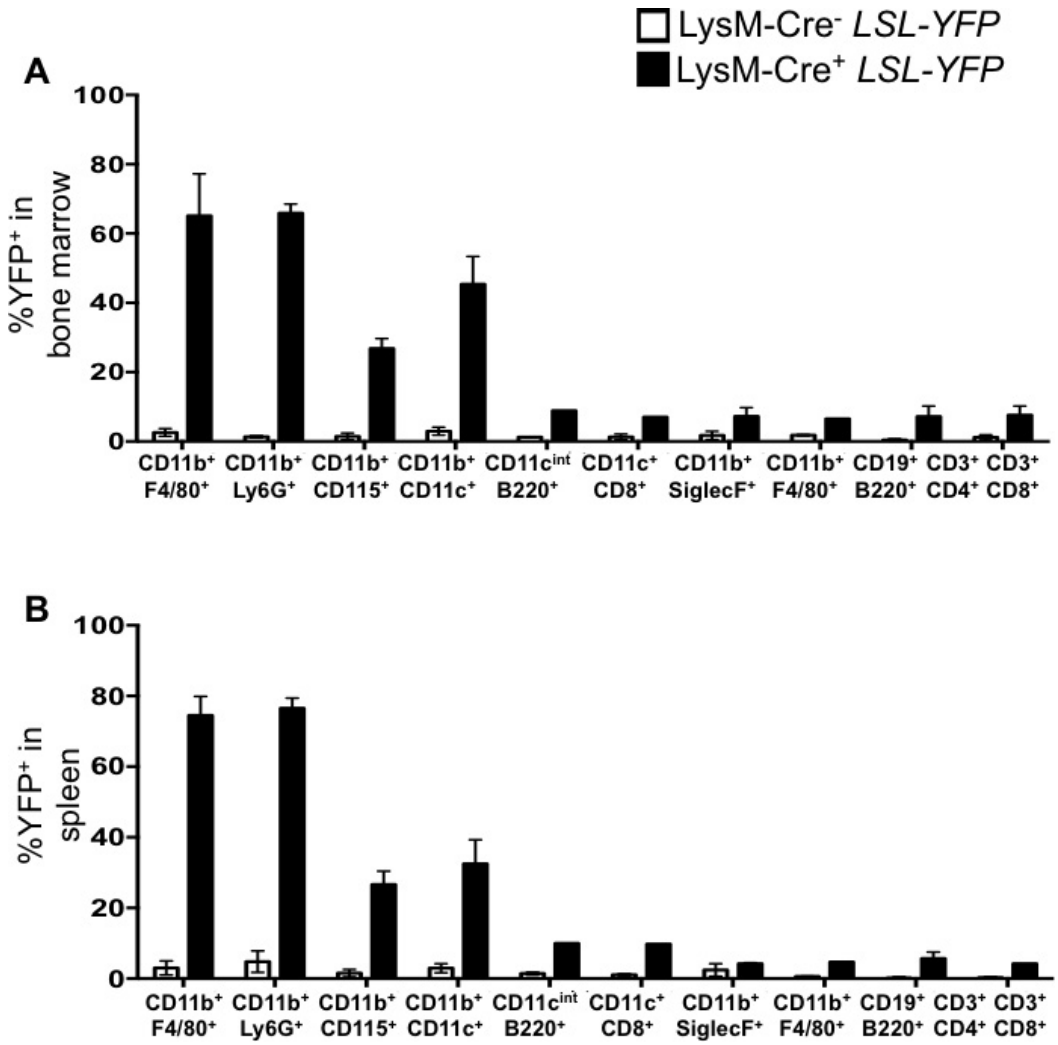

Extended Data Figure 1 | LysM-Cre recombinase activity *in vivo*. **a**, **b**, Bone marrow (**a**) and spleen (**b**) were obtained from wild-type and LysM-Cre$^+$ LSL–YFP reporter mice (R26-stop-EYFP) at 8 weeks of age and flow cytometry was performed to examine expression of YFP in the following cellular populations: macrophages (CD11b$^+$ F4/80$^+$), neutrophils (CD11b$^+$ Ly6G$^+$), monocytes (CD11b$^+$ CD115$^+$), conventional dendritic cells (CD11b$^+$ CD11c$^+$), plasmacytoid dendritic cells (CD11c^{int} B220$^+$), CD8α^+ dendritic cells (CD11c$^+$ CD8α^+), eosinophils (CD11b$^+$ SiglecF$^+$), B cells (CD19$^+$ B220$^+$), CD4$^+$ T cells (CD3$^+$ CD4$^+$), and CD8$^+$ T cells (CD3$^+$ CD8$^+$). Error bars represent s.d. ($n = 4$).

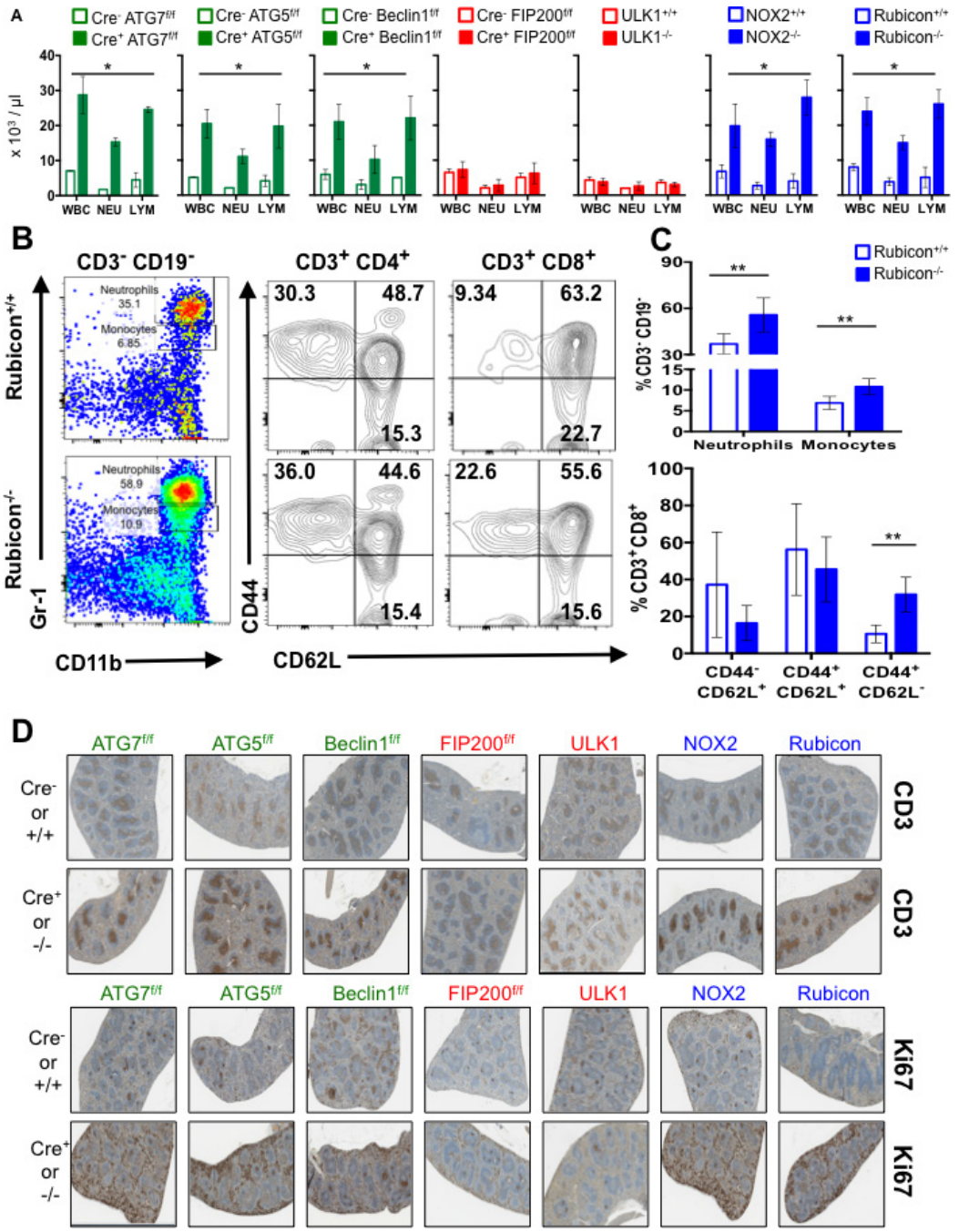

Extended Data Figure 2 | Mice with LAP deficiencies display symptoms of immune activation. a, Wild-type and deficient littermates were co-housed and aged for 52 weeks at SJCRH. Whole blood was collected at 52 weeks and analysed for differential blood count. Error bars represent s.d. LYM, lymphocytes; NEU, neutrophils; WBC, white blood cell s. **b**, **c**, Peripheral blood from *Rubcn*$^{+/+}$ and *Rubcn*$^{-/-}$ animals aged 52 weeks was analysed for immune cell populations. Neutrophils (singlets/CD3$^-$ CD19$^-$/Gr-1^{hi} CD11b$^+$), monocytes (singlets/CD3$^-$ CD19$^-$/Gr-1^{int} CD11b$^+$), activated T cells (singlets/CD3$^+$ CD4$^+$/CD44$^+$ CD62L$^-$ and singlets/CD3$^+$ CD8$^+$/CD44$^+$ CD62L$^-$), and central memory T cells (singlets/CD3$^+$ CD4$^+$/CD44$^+$ CD62L$^+$ and singlets/CD3$^+$ CD8$^+$/CD44$^+$ CD62L$^+$) were analysed and quantified. Error bars represent s.d. ($n = 5$, $^{**}P < 0.05$, Student's *t*-test). **d**, Spleens from wild-type and deficient littermates aged for 52 weeks were stained for anti-CD3 (top) or Ki67 (bottom) using immunohistochemistry. Representative images (original magnification, ×2.5) are shown ($n = 4$ per genotype). Error bars represent s.d. The colour scheme throughout represents LAP-deficient, autophagy-deficient genotypes (green), autophagy-deficient, LAP-sufficient (red), and autophagy-sufficient, LAP-deficient (blue).

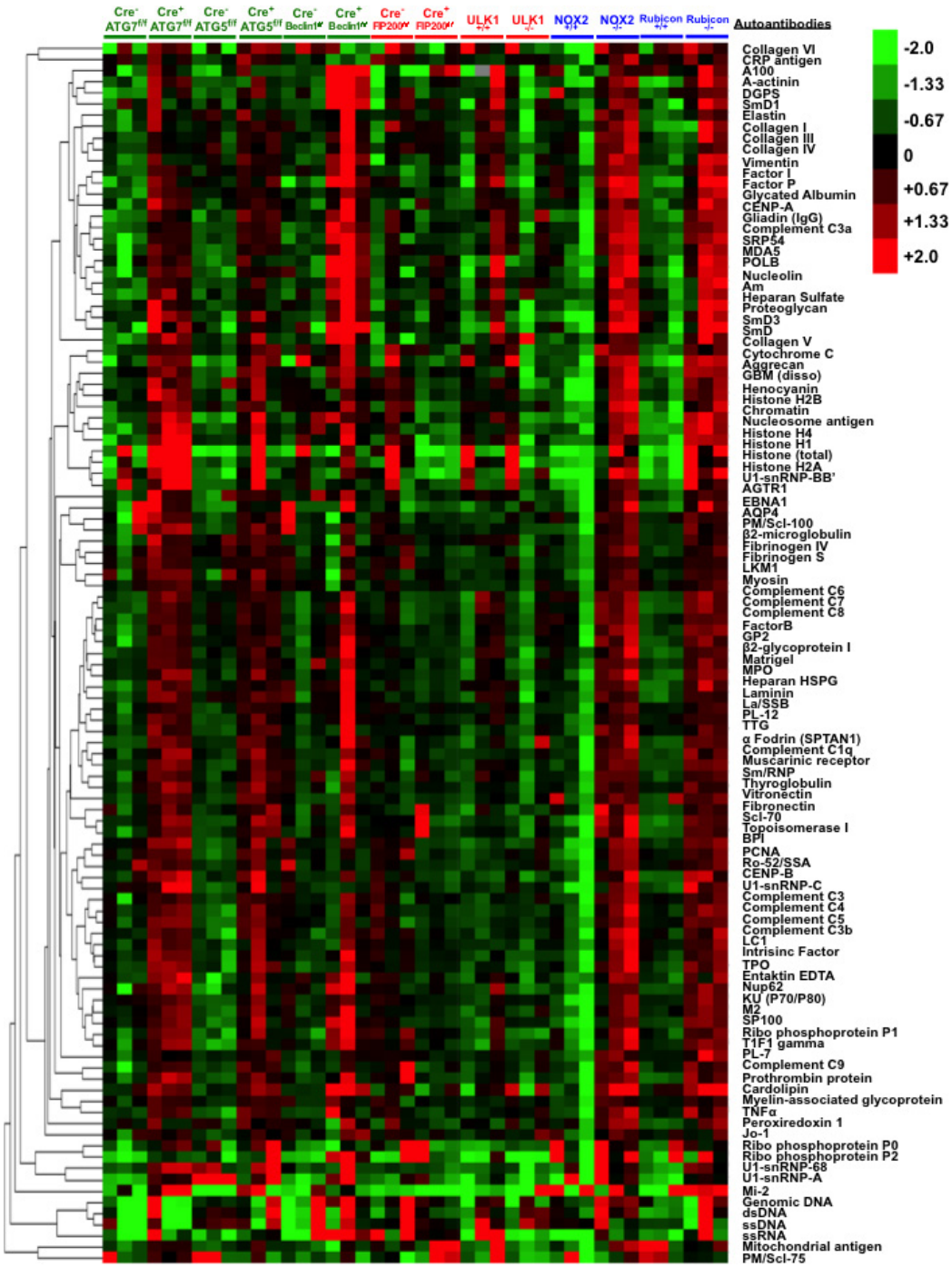

Extended Data Figure 3 | Mice with LAP deficiencies display increased levels of circulating autoantibodies. Serum from animals aged 52 weeks at SJCRH was analysed for autoantigens commonly associated with autoimmune and autoinflammatory disorders. The background subtracted signal intensity of each autoantigen was normalized to the average intensity of the total mouse IgG, which was included on the array as an internal control. IgG autoantibodies are shown, in triplicates per genotype.

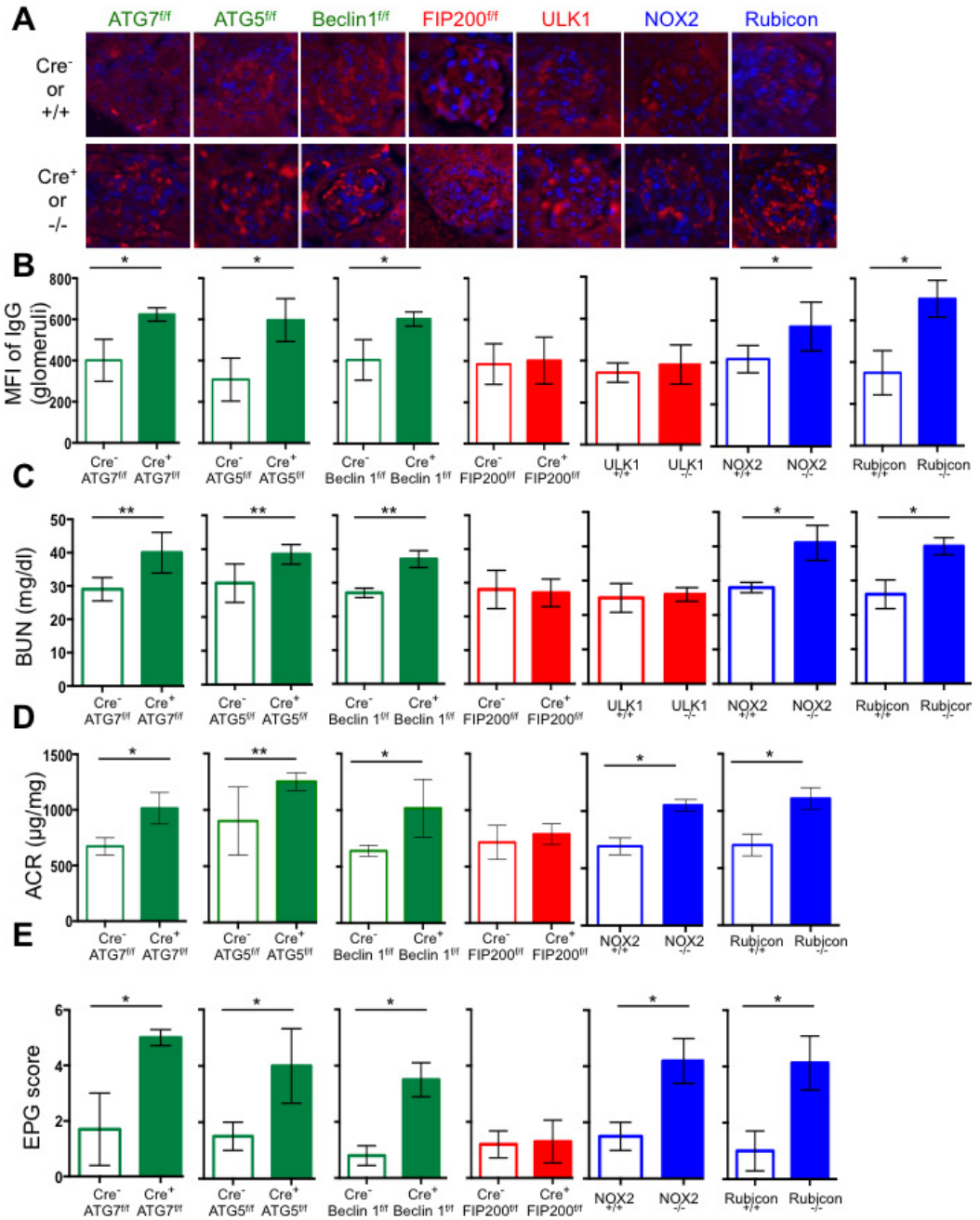

Extended Data Figure 4 | Mice with LAP deficiencies display kidney pathology. a, **b**, Wild-type and deficient littermates were co-housed and aged for 52 weeks at SJCRH. At 32 weeks, kidneys were obtained and stained for anti-IgG (red) and DAPI (blue) (**a**). Original magnification, ×100. MFI of anti-IgG staining in the glomeruli was calculated using Slidebook6 software (**b**). Error bars represent s.d. ($n > 15$ glomeruli per genotype, $^*P < 0.001$, Student's *t*-test). **c**, At 52 weeks, serum was collected and analysed for blood urea nitrogen (BUN). **d**, At 52 weeks, urine was collected, and proteinuria was calculated as the ratio of albumin to creatinine (ACR). Error bars represent s.d. ($n > 4$ per genotype, $^*P < 0.001$, $^{**}P < 0.05$). **e**, At 52 weeks, kidneys were obtained and stained for haematoxylin and eosin. Kidneys were scored blindly for endocapillary proliferative glomerulonephritis (EPG) on a scale of 1 (no damage) to 5 (clear damage). For histological assessment, at least 24 glomeruli were evaluated for each genotype. Error bars represent s.d. ($^*P < 0.001$, Student's *t*-test).

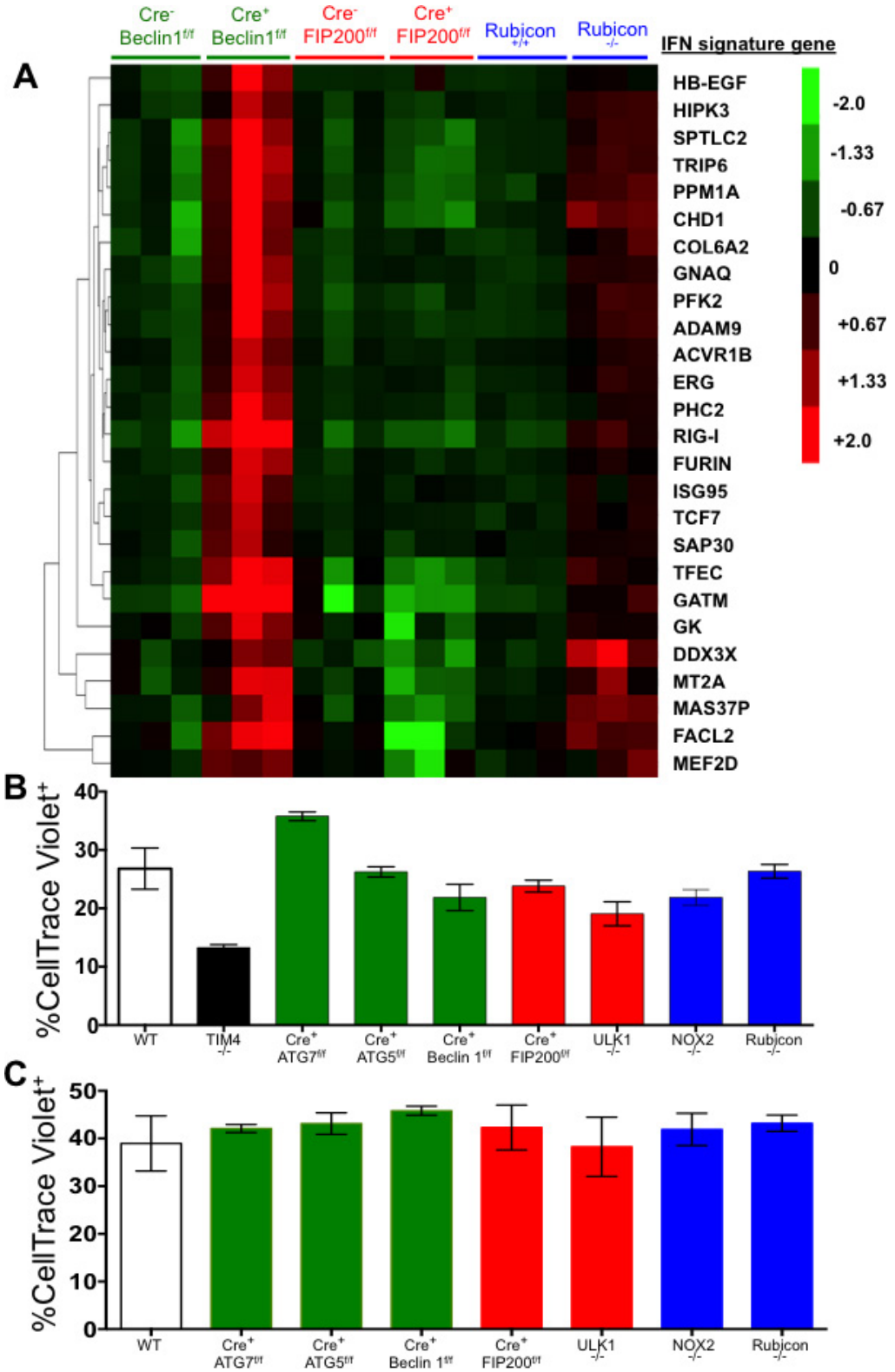

Extended Data Figure 5 | Mice with LAP deficiencies display increased expression of the IFN signature but normal phagocytic capacity. **a**, Wild-type and deficient littermates were co-housed and aged for 52 weeks at SJCRH. RNA was extracted from 52-week-old spleens and analysed for expression of genes associated with the IFN signature using Nanostring technology. Heatmap of Nanostring counts from the top 26 regulated genes in the IFN signature are shown in triplicate per genotype. **b**, UV-irradiated wild-type (WT) thymocytes were stained with CellTrace Violet and co-cultured (5:1) with bone-marrow-derived macrophages from wild-type and deficient genotypes for 45 min. Percentage phagocytosis (%CellTrace Violet$^+$) was quantified by flow cytometry (singlets/GFP$^+$ CellTrace Violet$^+$). **c**, Wild-type and deficient littermates were co-housed and aged for 52 weeks at SJCRH. Peritoneal macrophages were isolated after 3 days of intra-peritoneal injection of thioglycolate. UV-irradiated wild-type thymocytes were stained with CellTrace Violet and co-cultured (2:1) with peritoneal macrophages from wild-type and deficient genotypes for 1 h. Phagocytic efficiency (singlets/CellTrace Violet$^+$/F4/80$^+$) was quantified by flow cytometry (%CellTrace Violet$^+$). Error bars represent s.d. Data shown are representative of two independent experiments.

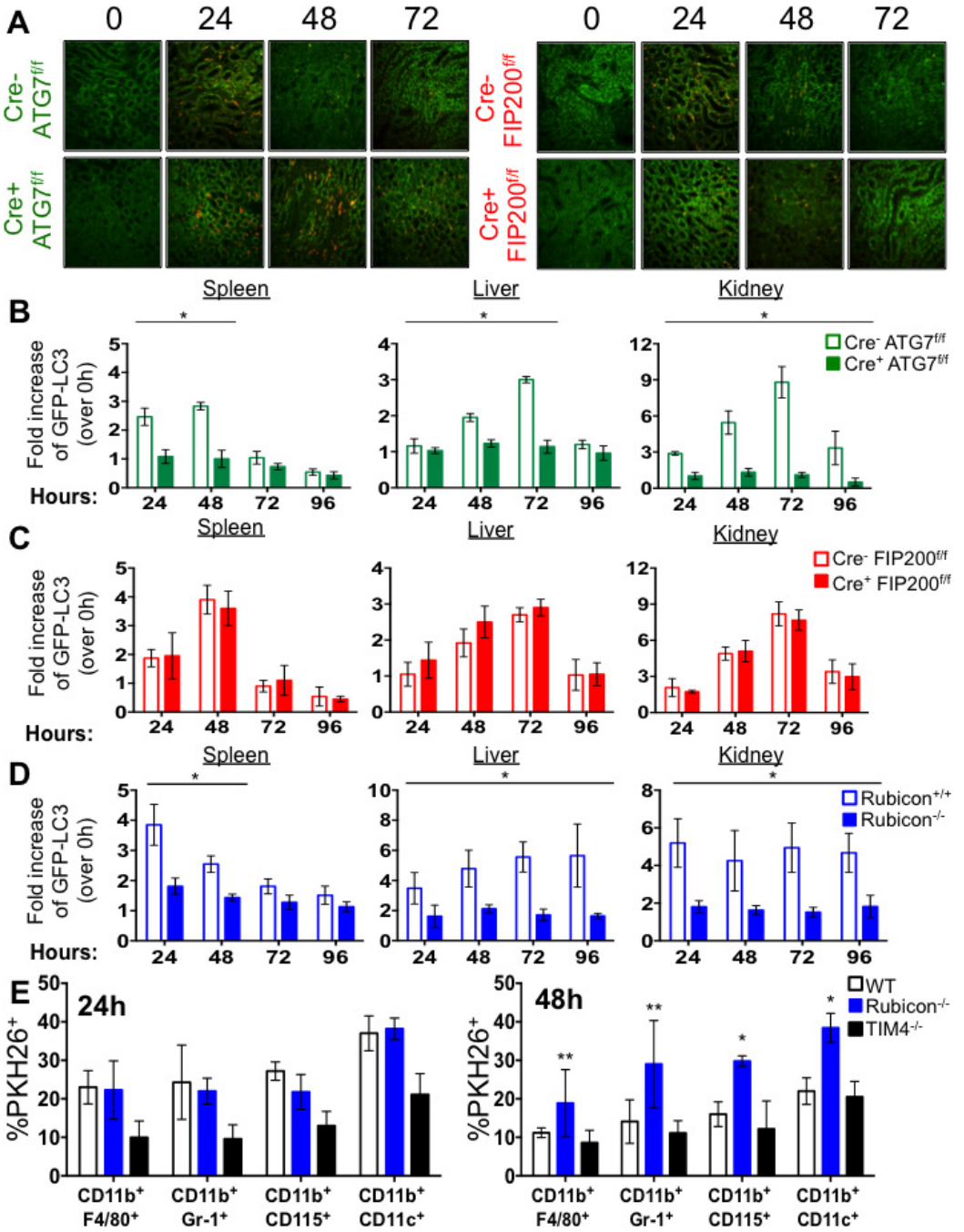

Extended Data Figure 6 | Mice with LAP deficiencies display defective clearance of engulfed, dying cells. a, 1×10^7 PKH26-labelled UV-irradiated wild-type thymocytes were injected intravenously into Cre$^-$ *Atg7*$^{f/f}$, Cre$^+$ *Atg7*$^{f/f}$, Cre$^-$ *Fip200*$^{f/f}$, or Cre$^+$ *Fip200*$^{f/f}$ animals (all GFP–LC3$^+$). Presence of labelled, apoptotic thymocytes was measured in kidney sections at 0, 24, 48, 72 and 96 h after transfer. Red cells are PKH26-labelled apoptotic thymocytes, and the kidney tissue is GFP–LC3. Representative images (original magnification, ×40) from two independent experiments are shown. **b**–**d**, Co-localization of lipidated GFP–LC3-II with engulfed dead cells was analysed by flow cytometry using digitonin treatment of spleen, liver and kidney of Cre$^-$ and Cre$^+$ *Atg7*$^{f/f}$ mice (**b**), Cre$^-$ and Cre$^+$ *Fip200*$^{f/f}$ mice (**c**), and *Rubcn*$^{+/+}$ and *Rubcn*$^{-/-}$ mice (**d**) at the indicated time points. **e**, 1×10^7 PKH26-labelled UV-irradiated wild-type thymocytes were injected intravenously into wild-type, *Rubcn*$^{-/-}$, or *Tim4*$^{-/-}$ animals. After 24 and 48 h, spleens were collected and stained with fluorescently conjugated surface markers for macrophages (CD11b$^+$ F4/80$^+$), neutrophils (CD11b$^+$ Gr-1$^+$), monocytes (CD11b$^+$ CD115$^+$), and dendritic cells (CD11b$^+$ CD11c$^+$). Phagocytic efficiency of each cell type (singlets/cell surface markers$^+$/PKH26$^+$) was quantified by flow cytometry (percentage PKH26). Data shown are representative of two independent experiments. Error bars represent s.d. (**$P < 0.05$, *$P < 0.001$, Student's *t*-test). The colour scheme represents LAP-deficient, autophagy-deficient genotypes (green), autophagy-deficient, LAP-sufficient (red), autophagy-sufficient, LAP-deficient (blue), and *Tim4*$^{+/+}$ and *Tim4*$^{-/-}$ (black).

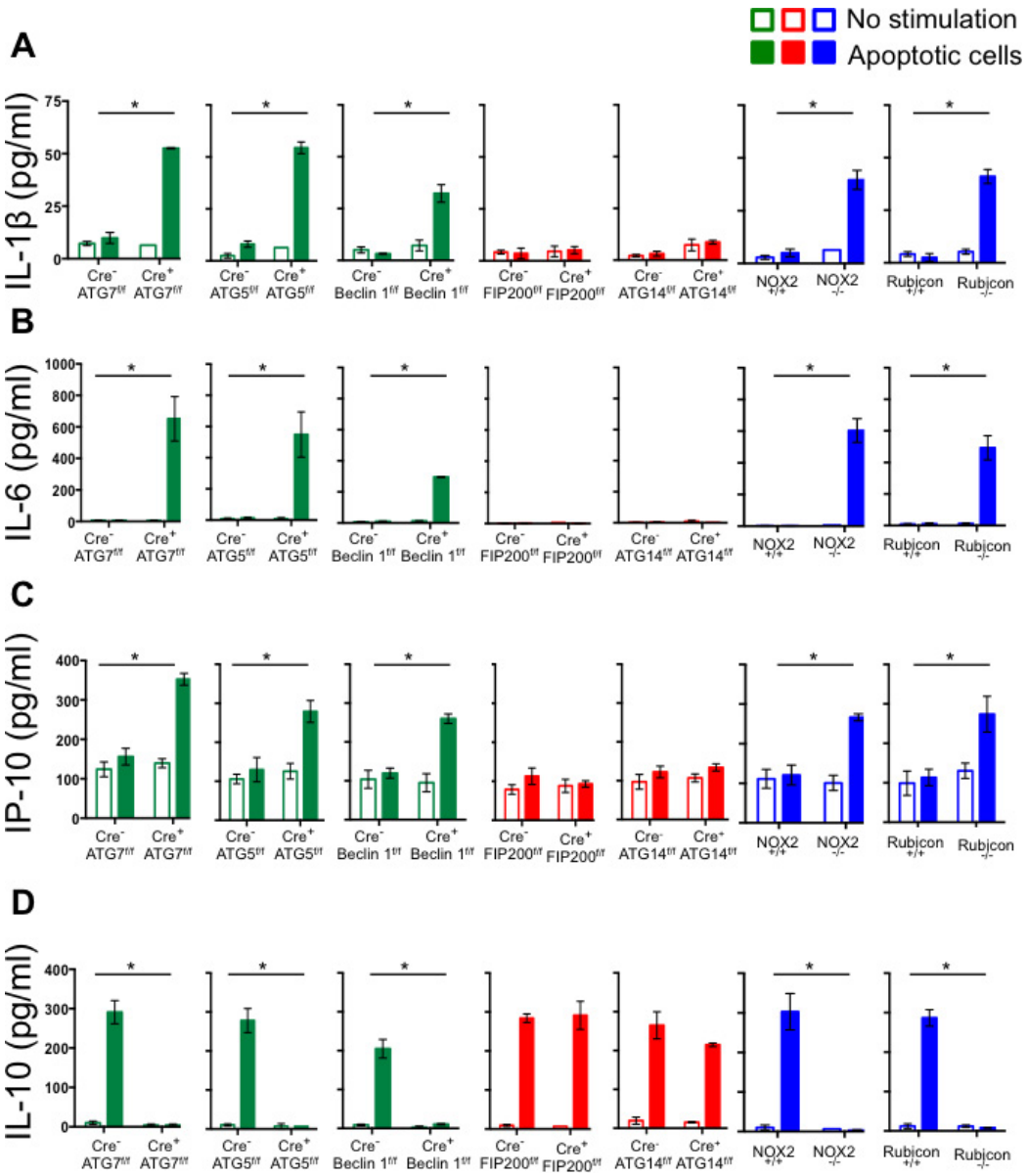

Extended Data Figure 7 | LAP is required for the anti-inflammatory response to apoptotic cell engulfment *in vitro*. **a**–**d**, UV-irradiated wild-type thymocytes were co-cultured with bone-marrow-derived macrophages from wild-type and deficient genotypes. Supernatant was collected at 24 h and analysed for IL-1β (**a**), IL-6 (**b**), IP-10 (**c**), and IL-10 (**d**) using Luminex technology. Error bars represent s.d. ($n = 4$, $^*P < 0.001$, Student's *t*-test). The colour scheme represents LAP-deficient, autophagy-deficient genotypes (green), autophagy-deficient, LAP-sufficient (red), autophagy-sufficient, and LAP-deficient (blue).

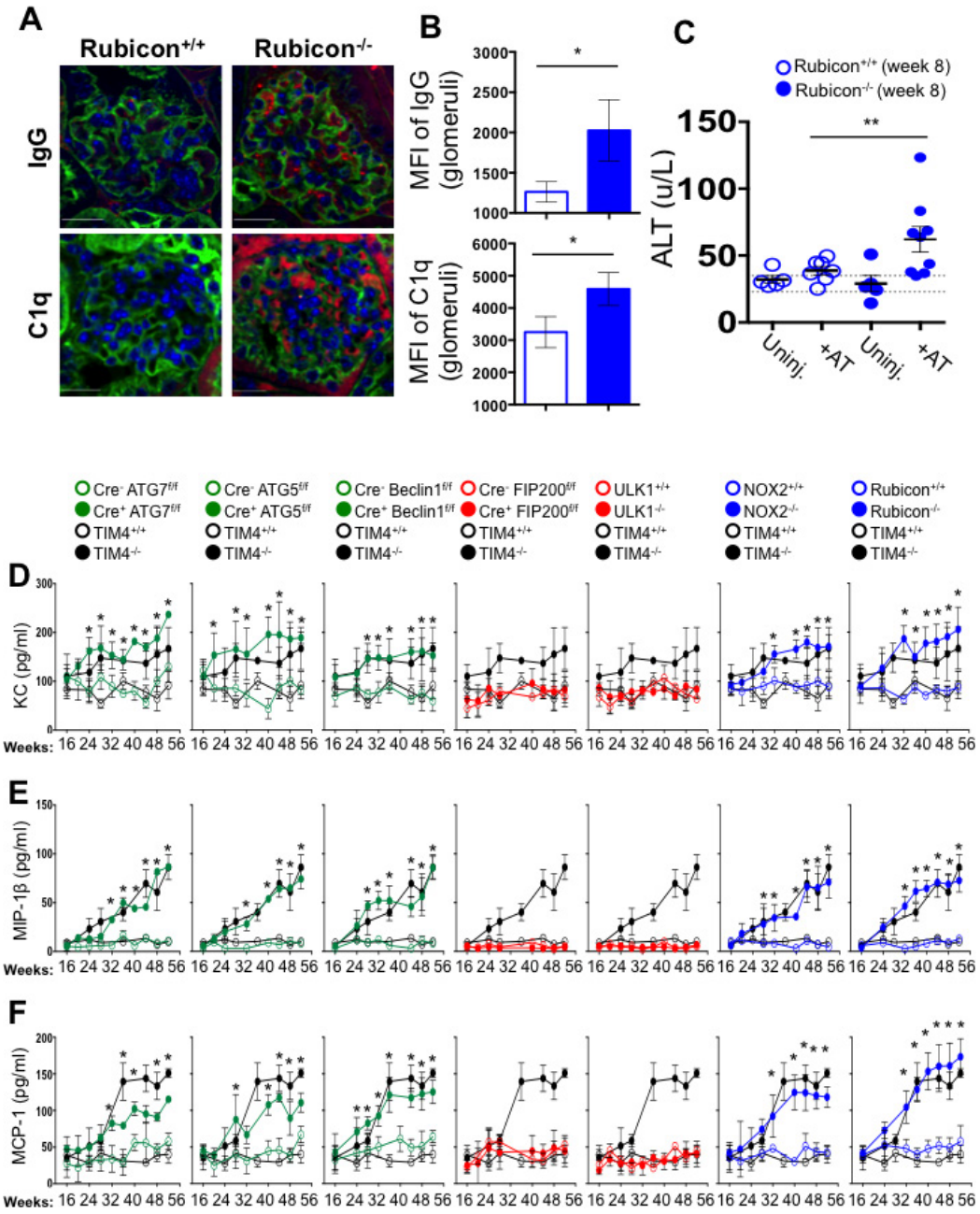

Extended Data Figure 8 | Mice with LAP deficiencies display symptoms of an autoinflammatory disorder. a–c, 2×10^7, UV-irradiated wild-type thymocytes were injected intravenously for 8 consecutive weeks into *Rubcn*$^{+/+}$ or *Rubcn*$^{-/-}$ animals (aged 6 weeks). After 8 weeks, kidneys were obtained and stained with DAPI (blue), wheat germ agglutinin (green), anti-IgG (red, top) and anti-C1q (red, bottom) (**a**). Original magnification, ×100. MFI of anti-IgG (top) and anti-C1q (bottom) staining in the glomeruli was calculated using Slidebook6 software (**b**). Error bars represent s.d. ($n > 15$ glomeruli per genotype, $^*P < 0.001$, Student's *t*-test). After 8 weeks (week 8), serum was collected from uninjected and injected (+AT) animals (all 16 weeks of age) and analysed for alanine aminotransferase (ALT). Dots represent values from individual animals (**c**). Error bars represent s.e.m. ($^{**}P < 0.05$, Student's *t*-test). **d–f**, Wild-type and deficient littermates were co-housed and aged for 52 weeks at SJCRH. Serum was collected every 4 weeks and analysed for KC (**d**), MIP-1β (**e**), and MCP1 (**f**) using Luminex technology. Error bars represent s.d. The colour scheme throughout represents LAP-deficient, autophagy-deficient genotypes (green), autophagy-deficient, LAP-sufficient (red), and autophagy-sufficient, LAP-deficient (blue). Values for one cohort of *Tim4*$^{+/+}$ and *Tim4*$^{-/-}$ animals are shown for comparison in all cases (black) in **a–c**.

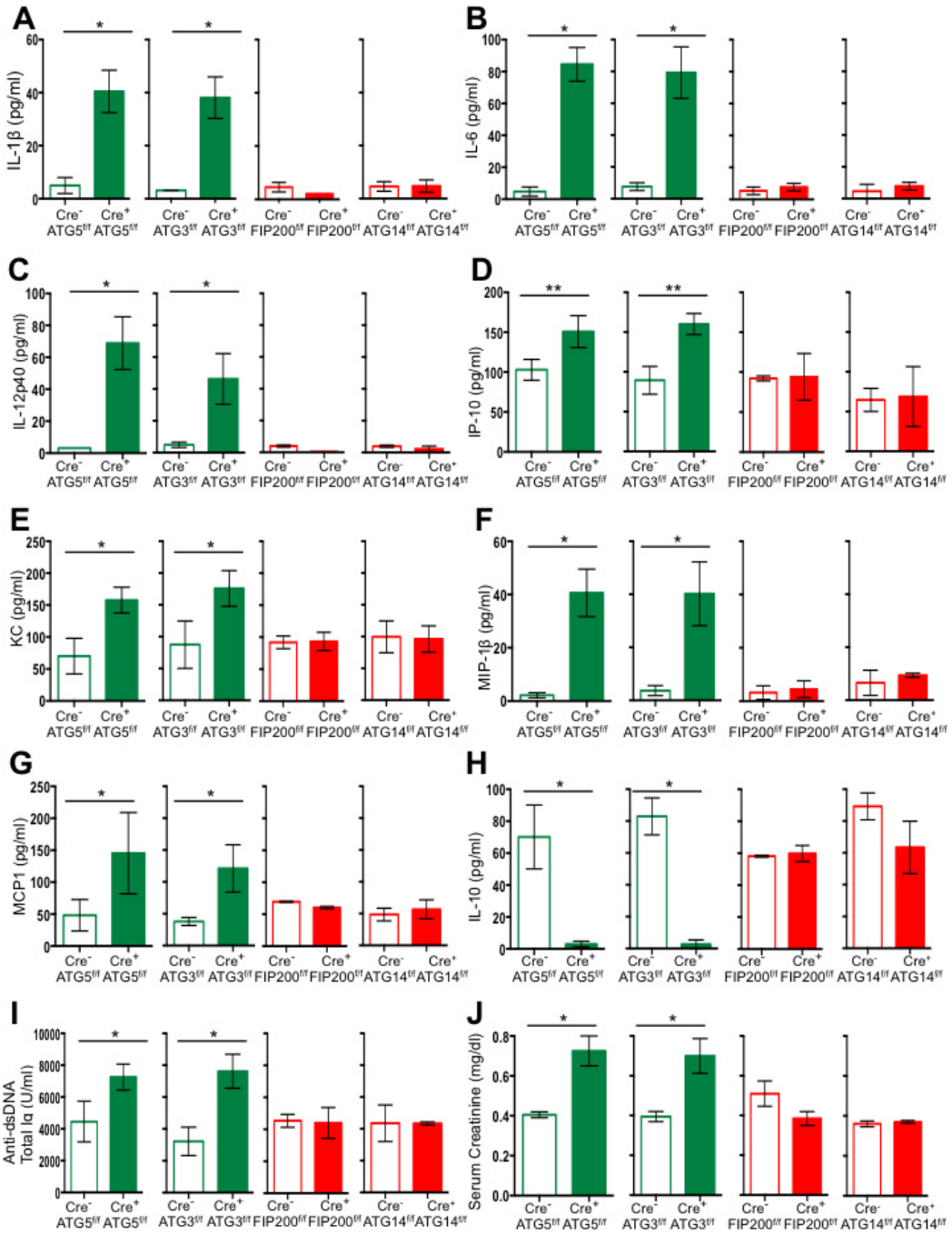

Extended Data Figure 9 | Mice with LAP deficiencies display symptoms of an autoinflammatory disorder. Wild-type and deficient littermates were co-housed and aged for 52 weeks at Washington University. Serum was collected at 48–52 weeks and analysed for IL-1β (**a**), IL-6 (**b**), IL-12p40 (**c**), IP-10 (**d**), KC (**e**), MIP-1β (**f**), MCP1 (**g**), and IL-10 (**h**) using Luminex technology. Serum was analysed for anti-dsDNA antibodies (total Ig (**i**) and creatinine (**j**)). Error bars represent s.d. (**$P < 0.001$, Student's *t*-test). The colour scheme throughout represents LAP-deficient, autophagy-deficient genotypes (green) and autophagy-deficient, LAP-sufficient (red).

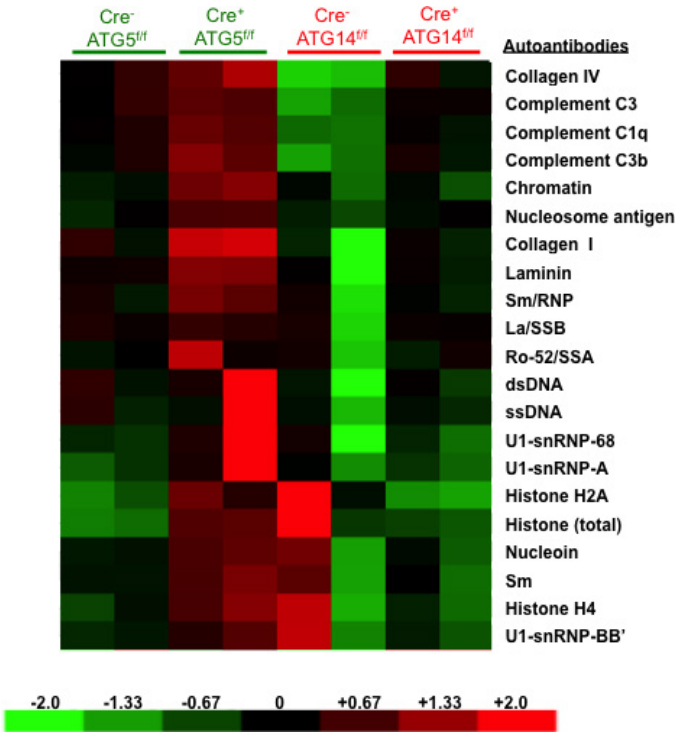

Extended Data Figure 10 | Mice with LAP deficiencies display increased levels of circulating autoantibodies. Serum from animals aged 52 weeks at Washington University was analysed for autoantigens commonly associated with autoimmune and autoinflammatory disorders. IgG autoantibodies are shown, in duplicates per genotype.